

Dear Author,

Please, note that changes made to the HTML content will be added to the article before publication, but are not reflected in this PDF.

Note also that this file should not be used for submitting corrections.



Contents lists available at ScienceDirect

Journal of Inorganic Biochemistry

journal homepage: www.elsevier.com/locate/jinorgbio

Q1 Alkynyl gold(I) phosphane complexes: Evaluation of structure–activity-relationships for the phosphane ligands, effects on key signaling proteins and preliminary in-vivo studies with a nanoformulated complex

Q2 Vincent Andermark^{a,b}, Katrin Göke^{b,c}, Malte Kokoschka^{d,e}, Mohamed A. Abu el Maaty^f, Ching Tung Lum^{g,h}, Taotao Zou^{g,h}, Raymond Wai-Yin Sun^{g,h}, Elisabet Aguilóⁱ, Luciano Oehninger^{a,b}, Laura Rodríguezⁱ, Heike Bunjes^{b,c}, Stefan Wölfl^f, Chi-Ming Che^{g,h}, Ingo Ott^{a,b,*}

^a Institute of Medicinal and Pharmaceutical Chemistry, Technische Universität Braunschweig, Beethovenstrasse 55, 38106 Braunschweig, Germany

^b PVZ – Center of Pharmaceutical Engineering, Franz-Liszt-Straße 35A, 38106 Braunschweig, Germany

^c Institute of Pharmaceutical Technology, Technische Universität Braunschweig, Mendelssohnstrasse 1, 38106 Braunschweig, Germany

^d Gilead Sciences & IOCB Research Center, Department of Computational Chemistry, Institute of Organic Chemistry and Biochemistry, Academy of Sciences of the Czech Republic, 16610 Prague 6, Czech Republic

^e Department of Physical Chemistry, Palacky University, 77146 Olomouc, Czech Republic

^f Department of Biology, Institut für Pharmazie und Molekulare Biotechnologie, Ruperto-Carola University of Heidelberg, Im Neuenheimer Feld 364, 69120 Heidelberg, Germany

^g State Key Laboratory of Synthetic Chemistry, Chemical Biology Center, Hong Kong

^h Department of Chemistry, The University of Hong Kong, Pokfulam Road, Hong Kong

ⁱ Departament de Química Inorgànica, Universitat de Barcelona, Martí i Franquès 1-11, 08028 Barcelona, Spain

ARTICLE INFO

Article history:

Received 1 October 2015

Received in revised form 8 December 2015

Accepted 28 December 2015

Available online xxx

Keywords:

Alkyne

Cancer

Formulation

Gold

Microarray

Xenograft

ABSTRACT

Gold alkynyl complexes with phosphane ligands of the type (alkynyl)Au(I)(phosphane) represent a group of 25 bioorganometallics, which has only recently been evaluated biologically in more detail. Structure–activity-relationships 26 studies regarding the residues of the phosphane ligand (P(Ph)₃, P(2-furyl)₃, P(DAPTA)₃, P(PTA)₃, P(Et)₃, 27 P(Me)₃) of complexes with a 4-ethynylanisole alkyne ligand revealed no strong differences concerning 28 cytotoxicity. However, a relevant preference for the heteroatom free alkyl/aryl residues concerning inhibition of 29 the target enzyme thioredoxin reductase was evident. Complex **1** with the triphenylphosphane ligand was selected 30 for further studies, in which clear effects on cell morphology were monitored by time-lapse microscopy. 31 Effects on cellular signaling were determined by ELISA microarrays and showed a significant induction of the 32 phosphorylation of ERK1 (extracellular signal related kinase 1), ERK2 and HSP27 (heat shock protein 27) in 33 HT-29 cells. Application of **1** in-vivo in a mouse xenograft model was found to be challenging due to the low sol- 34 ubility of the complex and required a formulation strategy based on a peanut oil nanoemulsion. 35

© 2015 Published by Elsevier Inc. 36

1. Introduction

Gold based therapeutics have a long tradition in medicine lasting 49 from ancient times over alchemy into modern ages [1–6]. While gold 50 and its salts have been used for hundreds to thousands of years, modern 51 research has witnessed the development of more sophisticated bioac- 52 tive complexes that contain several types of coordinated ligands (e.g. 53 thiolates [7,8], phosphanes [9–11], porphyrines [12], dithiocarbamates

[13,14], N-heterocyclic carbenes [15–18] or alkynes [19–25]) or 55 heterobimetallic species [26,27]. Currently, auranofin (see Fig. 1) and 56 other gold(I) species are registered drugs for the treatment of rheuma- 57 toid arthritis and strong evidence for their efficacy against different dis- 58 eases such as cancer or bacterial infections exists [2,28,29]. The renewed 59 interest in gold based metallodrugs has led to increasing efforts in un- 60 derstanding their biochemical mechanisms of drug action and in the ra- 61 tional development of improved pharmacologically active compounds 62 [5,6]. (See Scheme 1.)

Q4 A single mode of action for all gold complexes unlikely exists, how- 64 ever, strong and selective inhibition of the enzyme thioredoxin reduc- 65 tase (TrxR) has been demonstrated for many gold species and might 66 be in general of high relevance for the pharmacology of a large number 67 of gold metallodrugs. Further important biochemical characteristics ob- 68 served frequently with gold compounds include the inhibition of tumor 69 cell proliferation, the induction of apoptosis, antimitochondrial effects 70

Abbreviations: DFT, density functional theory; ERK, extracellular signal related kinase; FAK, focal adhesion kinase; GSK, glycogen synthase kinase; HSP, heat shock protein; MAPK, mitogen activated protein kinase; TOR, target of rapamycin; TrxR, thioredoxin reductase.

* Corresponding author at: Institute of Medicinal and Pharmaceutical Chemistry, Technische Universität Braunschweig, Beethovenstrasse 55, 38106 Braunschweig, Germany.

E-mail address: ingo.ott@tu-bs.de (I. Ott).

<http://dx.doi.org/10.1016/j.jinorgbio.2015.12.020>

0162-0134/© 2015 Published by Elsevier Inc.

Please cite this article as: V. Andermark, et al., Alkynyl gold(I) phosphane complexes: Evaluation of structure–activity-relationships for the phosphane ligands, effects on key s..., J. Inorg. Biochem. (2015), <http://dx.doi.org/10.1016/j.jinorgbio.2015.12.020>

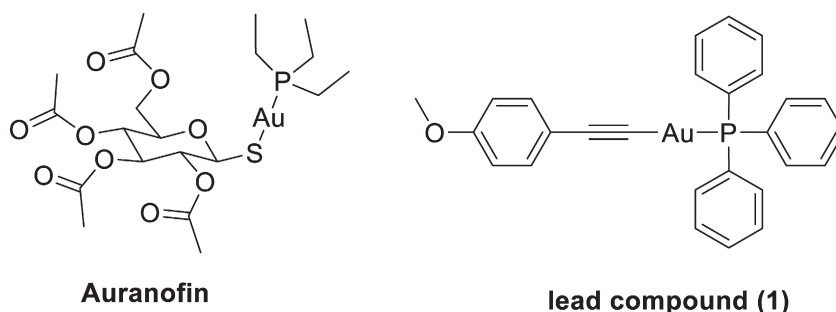


Fig. 1. The Au(I)(phosphane)thiolate complex auranofin and the (alkynyl)Au(I)(phosphane) complex **1**.

or the increased formation of reactive oxygen species. However, stability of the ligands coordinated to gold is a critical issue and triggers a high demand for gold complexes with stably coordinated ligands. Enhanced stability might be reached by the use of carbene ligands with the formation of organometallic gold species.

In this context, we have recently reported on gold(I) complexes of the type (alkynyl)Au(I)(triphenylphosphane) that contain an anionic alkynyl group as well as a neutral phosphane ligand [19,30]. Such organometallic gold compounds promise an improved stability compared to the traditional gold drugs based on the relatively high bond dissociation energies around the gold center. Some of the studied complexes turned out to be very strong and selective inhibitors of TrxR, showed high anti-proliferative activity in tumor cells, influenced key parameters of tumor cell metabolism, and triggered anti-angiogenic effects at non-toxic concentrations in zebrafish embryos [19].

Motivated by these encouraging biological properties, we selected a highly active complex of our previous report as a lead compound for further studies [19]. In the present study, the phosphane ligands were varied with the aim to establish possible structure–activity–relationships, and further biological properties were evaluated including effects on cellular signaling and in-vivo studies using a xenograft animal model.

1.1. Chemistry

Complexes **1–6** were prepared by reacting 4-ethynylanisole with the respective chlorido-gold(I)phosphane under basic conditions. The complexes were isolated and purified by filtration and washed as appropriate.

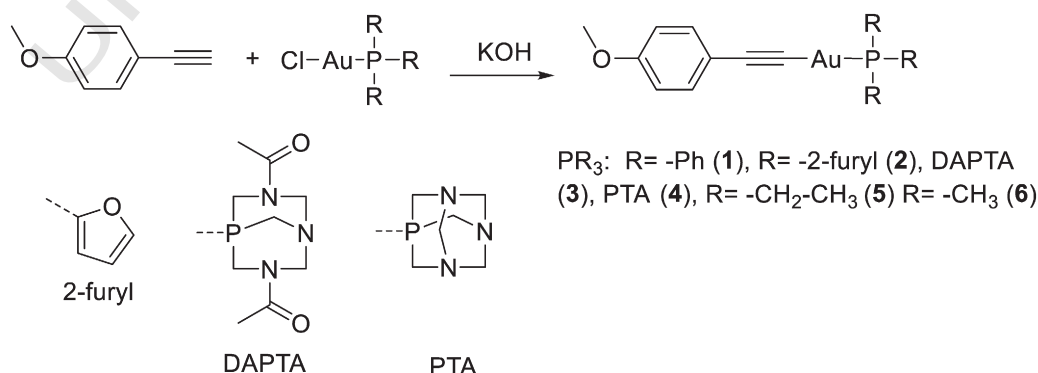
Complex formation and identity was clearly confirmed by the absence of the terminal hydrogen signal of the alkyne, the presence of the M^+ signal in mass spectrometry, and singlet resonances in ^{31}P -NMR spectra. ^{13}C -NMR spectra were taken (with the exception of complex **4**), however, the very low signal intensities of the alkyne carbons

did not allow a complete spectroscopic evaluation of these spectra. The high purities necessary for biological evaluation were confirmed by elemental analyses (deviations below 0.3% from the theoretical values).

Based on the below described biological screening, complex **1** was selected for further studies and in this context the synthesis procedure of **1** was stepwise improved resulting in a yield of 58%. The improved method for the synthesis of **1** is described in more detail in the [Experimental section](#).

Density Functional Theory (DFT) at the RI-PBE-D3/def2-TZVPP COSMO level was used to calculate geometries of all complexes in vacuo and in water. As example the calculated solution structure of **1** is shown in [Fig. 2](#).

Subsequently high level post-SCF calculations were used to determine bond dissociation energies of the ligand–gold bonds. This allows estimating the influence of ligand variations on the stability of their coordination bonds. We chose the LPNO–CEPA [31] method and a mixed def2-QZVP/def2-TZVP [32] basis set to perform bond dissociation scans. The LPNO–CEPA method was recently introduced by Neese et al. and combines a high speed with an accuracy, intermediate to CCSD and the current gold standard CCSD(T) [31]. Our calculations showed for both the C–Au and the P–Au bonds high bond dissociation energies in the range of 67.72–74.02 Kcal/mol for the C–Au bond and 48.00–58.73 Kcal/mol for the P–Au bond. These differences are more pronounced than those seen in an earlier study on alkynyl gold(I) complexes [19], where the differences were in the range of 2 kcal/mol for the C–Au bonds and 0.5 kcal/mol for the P–Au bonds. The larger differences of 7.6 kcal/mol for the C–Au bonds and 10.7 kcal/mol for the P–Au bonds are likely to originate from the larger differences in the electron donating ability of the used alkynyl ligands. A strengthening of the P–Au bond is observed with a weakening of the C–Au bond, as it was found for the C–Au bond of carbene gold(I) complexes upon variation of the opposing ligand [9,33].



Scheme 1. Synthesis of complexes **1–6**.

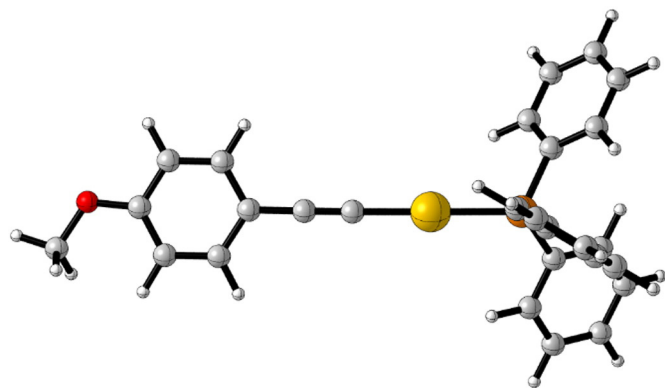


Fig. 2. Solution structure of complex 1 calculated by DFT.

Concerning the weaker P–Au bonds this indicates the following order of stability of the compounds: $2 < 3 < 4 < 1 < 6 < 5$. Noteworthy, the significantly highest values were determined for compounds **5** and **6** with ethyl and methyl residues, respectively.

1.2. Effects on cell proliferation, TrxR and cell morphology

The antiproliferative effects of complexes **1–6** were evaluated in HT-29 colon carcinoma and MDA-MB-231 breast adenocarcinoma cells. The obtained IC_{50} values were in a rather narrow range of 1–5 μM (2.6–5.0 μM in HT-29 cells, and 1.1–3.8 μM in MDA-MB-231 cells), and thus did not allow clear conclusions concerning structure–activity–relationships. The most active compound, however, was **5**, which afforded the lowest IC_{50} values in both cell lines indicating some preference for the triethylphosphane ligand concerning cytotoxicity.

The disulfide reductase enzyme TrxR is an established target for gold metallo drugs [34–36]. As expected, complexes **1–6** were efficient inhibitors of TrxR with IC_{50} values in the low nanomolar range. Compounds **1**, **5** and **6** with phenyl-, ethyl-, and methyl-substituted phosphane ligands were highly active (IC_{50} values of 0.05 and 0.06 μM , respectively) and complexes **2–4** with furyl-, DAPTA and PTA containing phosphanes also afforded appreciable IC_{50} values. However, **2–4** were significantly less active against TrxR than **1**, **5** and **6** (see Table 2). (See Table 1.)

Since the differences in cytotoxicity between these most active TrxR inhibitors (**1**, **5** and **6**) were small and previous studies had indicated interesting additional biological properties of complex **1** (e.g. anti-angiogenic properties, effects on mitochondria), this compound was selected as a well investigated example for further studies [19].

In order to check for possible tumor selectivity, the cytotoxicity against non-tumor L-929 mouse connective tissue fibroblasts and RC-124 human kidney cells was evaluated. IC_{50} values of $3.3 \pm 1.0 \mu\text{M}$ in L-929 cells and $1.5 \pm 0.2 \mu\text{M}$ in RC-124 cells, respectively, were obtained. This high antiproliferative activity against non-tumor cell lines indicates that compound **1** does not show selectivity for tumor tissue.

Microscopic live cell imaging allows monitoring of morphological changes in drug exposed cells under cell culture conditions. In these experiments RC-124 or HT-29 cells were grown until at least 20% confluency before **1** was added and pictures were taken every hour for 96 h (see Fig. 3 and video files of the supporting information).

Whereas untreated RC-124 control cells showed a continuous extension of the cell layer leading to confluency, cells treated with 1.5 μM of **1** experienced major morphological alterations within the first 12 h of exposure. This was most obvious after 6–10 h of incubation when the cells were strongly deformed compared to the untreated control and rounded up. With longer exposure cell growth still was maintained, however, cell morphology was substantially affected as evident by an elongated shape of the cells.

In contrast analogous experiments using HT-29 cells exposed to 10 μM of **1** remained morphologically little affected for more than

30 h, after which obvious cell death occurred as evidenced by a detachment and rounding up of the cells. This effect was not reversible and cells completely detached over extended exposure.

1.3. ELISA microarray studies

In order to gain more insights into the mechanisms of **1** on the cellular level several important key signaling proteins were measured in their phosphorylated states in HT-29 colon cancer cells (see Fig. 4). For this purpose an ELISA microarray assay was used, which had previously been developed and applied [37]. Complex **1** was administered at concentrations of 5.0 μM and 10 μM , and measurements were done over a period of 5 h.

A highly significant and persistent activation of the important mitogen activated protein kinases (MAPK) phospho-ERK1 (phosphorylated extracellular signal related kinase 1) and phospho-ERK2 was clearly observed. Both kinases play a key role in the MAPK cascade and regulate diverse biological functions such as cell growth, differentiation and survival. Moreover, the chaperone HSP27 (heat shock protein 27) was strongly induced by 10 μM of **1**, and this can be interpreted as a response to cytotoxic stress caused by the compound. Low effects or absence of effects were noted for the phosphorylations of the focal adhesion kinase (FAK), the proto-oncogene Src, target of rapamycin (TOR), p70S6K, glycogen synthase kinase 3 β (GSK-3 β), Akt1, p38, and Chk2.

1.4. Formulation of 1 and preliminary animal studies

Initial experiments to prepare solutions or suspensions of **1**, which are suitable for administration purposes in mice, were done using oil or phosphate buffered saline. For this purpose the compound was dissolved in concentrations up to 0.2 mg/ μL in DMF, DMSO, PET (60% polyethylene glycol 400, 30% ethanol, 10% Tween 80) or Kolliphor EL and the resulting stock solutions were diluted up to 50-fold using phosphate buffered saline or oil. However, these attempts did not afford suitable solutions/suspensions since visually non-homogenous precipitates were obtained upon dilution.

Accordingly, several pharmaceutical formulations were screened to increase the solubility of complex **1**. The nine used formulations included nanoemulsions of various oils, mixed micelles, smectic nanoparticles and liposomes (see Experimental section) [38]. After incubation with an excess of **1** and removal of undissolved material, the amount dissolved in each carrier was preliminarily estimated (for details see supporting information) via atomic absorption spectroscopy (AAS) and for the three carriers with the best loading results, the gold content was exactly determined using AAS. These measurements yielded the following total concentrations of **1**: 0.017 mg/ml in Dynasan 112 nanoemulsion, 0.009 mg/ml in mixed micelles and 0.028 mg/ml in peanut oil nanoemulsion.

Accordingly, peanut oil nanoemulsions, which had dissolved the highest levels of **1**, were selected for the preliminary in-vivo studies. For these animal experiments a dedicated nanoemulsion formulation was prepared which was handled and bottled under aseptic conditions. Crushing complex **1** prior to incubation led to a higher drug load in this emulsion compared to the screening results (0.098 mg/ml).

Table 1

Estimated bond dissociation energies (bond elongation of 5 Å) and ratios between C–Au and P–Au bonds.

Compound	C–Au	P–Au	C/P
	Kcal/mol	Kcal/mol	
1 (–Ph)	72.05	53.21	1.35
2 (–2-furyl)	74.02	48.00	1.54
3 (DAPTA)	72.71	50.38	1.44
4 (PTA)	71.03	51.97	1.37
5 (ethyl)	67.72	58.73	1.15
6 (methyl)	68.63	57.68	1.19

Table 2
Antiproliferative effects in HT-29 and MDA-MB-231 cells and inhibition of TrxR expressed as IC₅₀ concentrations in micromolar (μM) units.

	HT-29	MDA-MB-231	TrxR
1 (R = -Ph)	5.0 [19]	2.4 ± 0.3	0.05 [19]
2 (R = -2-furyl)	4.5 ± 0.3	3.8 ± 0.4	0.92 ± 0.13
3 (R = -DAPTA)	3.3 ± 0.2	2.1 ± 0.2	0.12 ± 0.04
4 (R = PTA)	4.3 ± 0.3	2.5 ± 0.3	0.14 ± 0.04
5 (R = -CH ₂ -CH ₃)	2.6 ± 0.1	1.1 ± 0.1	0.06 ± 0.01
6 (R = -CH ₃)	4.2 ± 0.4	1.6 ± 0.1	0.05 ± 0.01

To study effects of this formulation of **1** in-vivo an established NCI-H460 xenograft model was used. A number of six doses (2.5 mg/kg) of formulated **1** were injected intratumorally at days 0, 2, 5, 7, 9 and 12. The tumor volumes were measured and mice were sacrificed after 14 days (see Figs. 5 and 6). However, the treatment was not effective as the tumor volumes did not reduce. Body weight changes in the treated group were not observed indicating that the application was well tolerated.

2. Conclusions

Gold alkynyl phosphane complexes can be prepared in a convenient one step procedure in high purities as required for biological and

pharmacological studies. Quantum chemical calculations indicated a higher stability for derivatives with short alkyl residues (methyl, ethyl) at the phosphane. The complexes trigger strong antiproliferative effects in tumor cells. However, as exemplified for complex **1**, their cytotoxicity was not selective for tumor cells. While the cytotoxic effects were largely independent of the residues at the phosphane (with a slight preference for the ethyl group), some structure–activity-relationships could be noted concerning TrxR inhibition indicating that alkyl/phenyl residues are preferred over those containing N/O heteroatoms.

Time-lapse video imaging showed that RC-124 kidney cells were affected strongly with the first hours of exposure to **1** and showed an elongated shape after longer incubation. Such phenomena might indicate interactions of **1** with components of the cell surface or extracellular matrix and interference with cell division. In contrast, HT-29 cells were affected morphologically after longer exposure resulting in an irreversible rounding-up and detachment of the cells. Altogether these observations show that the cytotoxic effects of **1** are dependent on the type of cell line and/or cell culture conditions. Of note, RC-124 cells were maintained in culture using gelatin-coated cell culture materials (see Experimental section) in order to improve adhesion to the surfaces and were treated with a lower dosage of **1** (1.5 μM) compared to HT-29 cells (10 μM) based on the results of the cytotoxicity assay. The effects of **1** on cell morphology and adherence are of interest considering our previous report on strong anti-angiogenic effects in zebrafish embryos at non-toxic concentrations [19]. Rounding up and cell detachment had also been reported

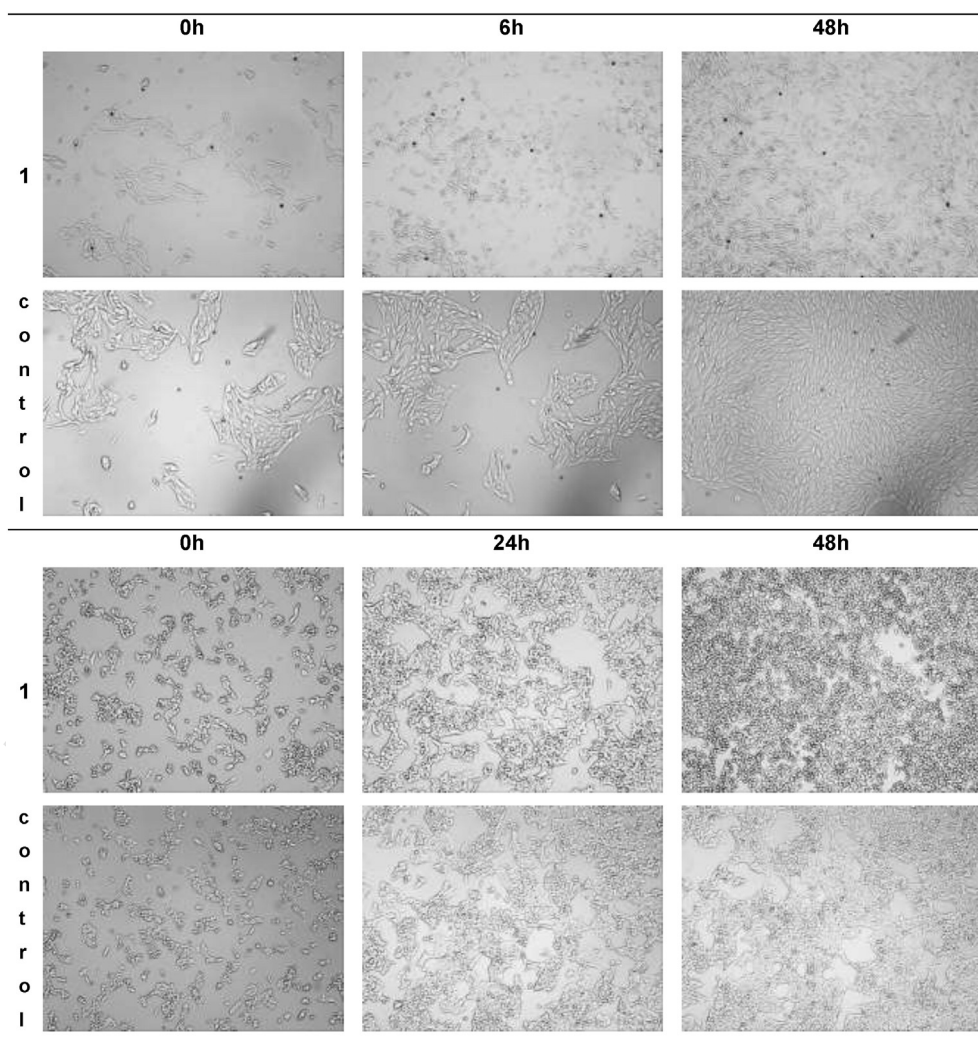


Fig. 3. Morphological changes in RC-124 (top) and HT-29 (bottom) cells. Cells were exposed to 1.5 μM (RC-124) or 10 μM (HT-29) of **1** and images were taken every hour over a period of 96 h. Time-lapse videos are provided as supporting information.

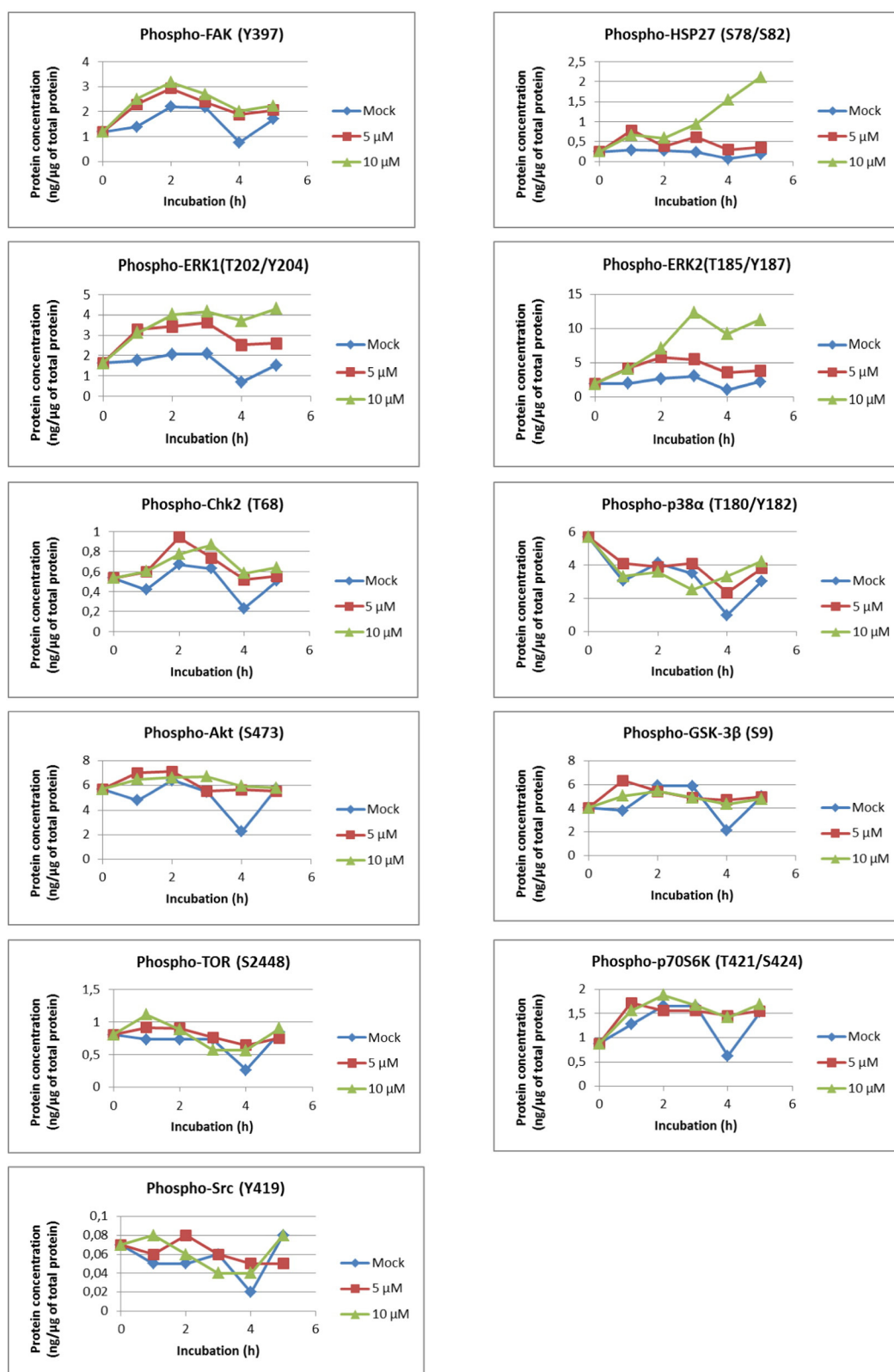


Fig. 4. ELISA microarray measurements of absolute phosphor-protein concentrations in HT-29 cells treated with 1. mock-treatment: solvent control (DMF).

280 for the gallium complex KP46, which caused a loss of integrin mediated
 281 cell adhesion [39]. Sensitivity against KP46 was found to be enhanced
 282 when cells were grown on collagen I, which is a major ligand for integrins
 283 [39]. Taken together, it can be speculated that some of the cytotoxic ef-
 284 fects of 1 – especially against the highly sensitive RC-124 cells grown

on gelatine – might in a similar manner be related to interference with
 cell surface proteins.

Further studies on 1 confirmed clear effects on cellular signaling in
 HT-29 cells with strong inductions of ERK1/2 and HSP27. In particular
 concerning the effects on ERK1 and ERK2 phosphorylation, 1 showed
 a similar pattern like previously studied phosphane containing gold

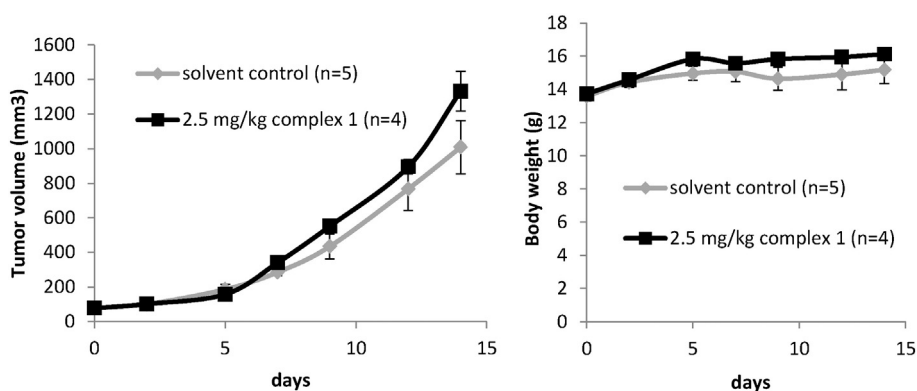


Fig. 5. Tumor volume (left) and body weight (right) in the NCI-H460 xenograft mice model.

complexes [40], but differed from a biscarbene gold(I) complex, which had not triggered ERK activation [41]. Strong induction of HSP27 phosphorylation had also been observed with the two other gold metallodrugs recently [40,41]. Small effects of **1** were noted on the phosphorylation of FAK in the investigated period of 5 h, which is in agreement with the observation that cell detachment of this cell line occurred only after extended exposure of more than 30 h.

Taken together with previous results [19,30] the organometallic alkynyl-gold(I)-phosphane center can be regarded as a useful organometallic pharmacophore, which can be incorporated into biologically active structures (e.g. coumarins [24] or naphthalimides [25]).

However, the in-vivo application of the model compound **1** experienced major difficulties related to the insufficient solubility of the complex in media used for injection. Nanoformulation of **1** in a peanut oil nanoemulsion resulted in a formulation suitable for injection purposes in mice. The low drug loading allowed a maximum dosage of 2.5 mg/kg, which was applied in a mouse xenograft model. The dosage was ineffective concerning tumor growth inhibition but was well tolerated. The inactivity might be the consequence of the low dosage applied or caused by an inefficient drug release from the formulation. Accordingly, further studies will be required to translate the promising in-vitro effects of alkynyl gold species into animal models. Such strategies to enhance the in-vivo efficacy need to address the solubility problems encountered with complex **1**. Improved pharmaceutical formulations of **1** appear very promising in this aspect as well as further structural optimizations leading to compounds with lower lipophilicity.

3. Experimental section

3.1. General

All reagents were obtained from Sigma-Aldrich (Switzerland) or Fluka Analytical. The purities of the synthesized compounds were confirmed by elemental analysis (Flash EA 1112, Thermo Quest) and differed less than 0.5% from the predicted values. ¹H NMR spectra, ¹³C NMR spectra and ¹⁹F NMR spectra were recorded using a Bruker AV II-400 or Bruker DRX-400 AS NMR spectrometer. Mass spectra were recorded on a Finnigan-MAT 95 spectrometer (ionization energy for EI-MS: 70 eV). For the absorption measurements in biological assays a Perkin Elmer 2030 Multilabel Reader VICTOR™ X4 was used.

3.2. Improved synthesis method for complex 1

100.0 mg (0.757 mmol) 1-ethynyl-4-methoxybenzene and 127.3 mg (2.270 mmol) KOH were dissolved in 20 ml methanol and stirred for 10 min. 374.7 mg (0.757 mmol) chlorido(tri-phenylphosphane)gold(I) were added to the solution forming a suspension. Dichloromethane was added dropwise to the solution until the solid was completely solubilized. The solution was stirred for 2 h

under light protection and afterwards stored for 72 h at -20°C . White crystals were formed during storage and were filtered off. The resulting solid was dissolved in CH_2Cl_2 and washed 2 times with water. The organic solvent was dried with NaSO_4 and then removed under reduced pressure. Yield: 58% (259.0 mg); elemental analysis (found/theor.): C(55.02/54.93), H(3.72/3.76) spectral data (NMR and MS spectra) were as reported before [19].

3.3. General procedure for complexes 2–6

1-ethynyl-4-methoxybenzene and KOH are dissolved in methanol or methanol/dichloromethane 2/1. After 10 min of stirring and complete solution of 1 equivalent of the respective chloridogold(I)phosphane is added and stirring at room temperature is continued under light protection (reaction time). After formation of an initial precipitate the mixture is stored at -20°C , the precipitate is isolated by filtration and, if necessary, purified by washing with water or methanol, and dried.

Complex **2**, [tri(2-furyl)phosphane][2-(4-methoxyphenyl)ethynyl]gold(I). General method: 18.9 mg (0.143 mmol) 1-ethynyl-4-methoxybenzene, 8.0 mg (0.143 mmol) KOH, 10 ml methanol, 66.4 mg (0.143 mmol) chloridogold(I)[tri(2-furyl)phosphane]; 2 h reaction time, 0 h at -20°C , yield 40 mg (50%) gray powder (m.p. $135\text{--}136^{\circ}\text{C}$); ¹H-NMR (CDCl_3): 3.73 (s, 3 H, OCH_3), 6.46 (m, 3 H, ArH), 6.75 (m, 2 H, ArH), 7.12 (m, 3 H, ArH), 7.39 (m, 2 H, ArH), 7.70 (m, 3 H, ArH); ¹³C-NMR (CDCl_3): 55.02 (OCH_3), 111.94 (d, $J = 8.9\text{ Hz}$, ArC), 113.92 (ArC), 125.02 (ArC) 132.65 (ArC), 151.02 (ArC), C \equiv C signals not observed; ³¹P-NMR (CDCl_3): -29.03 (s); MS(EI): 561.06 [M + H]⁺; elemental analysis [found/theor.]: C (44.83/45.02), H(2.79/2.88). Complex **3**, [tri[3,7-diacetyl-1,3,7-triaza-5-phosphabicyclo[3.3.1]nonane]phosphane][2-(4-methoxyphenyl)ethynyl]gold(I). General method: 15.7 mg (0.118 mmol) 1-ethynyl-4-methoxybenzene, 6.7 mg (0.118 mmol) KOH, 10 ml methanol + 5.0 ml dichloromethane, 54.8 mg (0.118 mmol) chloridogold(I)[tri[3,7-diacetyl-1,3,7-triaza-5-phosphabicyclo[3.3.1]nonane]phosphane]; 2 h reaction time (then concentrated in vacuum), 12 h at -20°C , yield 20 mg (30%) white powder; ¹H-NMR (CDCl_3): 1.99 (s, 3 H, COCH_3), 2.01 (s, 3 H, COCH_3), 3.68 (m, 1 H), 3.72 (s, 3 H, OCH_3), 3.93 (m, 3 H), 4.18 (m, 1 H), 4.49 (m, 1 H), 4.63 (m, 1 H), 4.80 (m, 1 H), 5.53 (m, 1 H), 5.63 (m, 1 H), 6.73 (m, 2 H, ArH), 7.30 (m, 2 H, ArH); ¹³C-NMR (CDCl_3): 21.25 (s, COCH_3), 21.52 (s, COCH_3), 39.59 (d, PCH_2N , $J = 26.9\text{ Hz}$), 44.79 (d, PCH_2N , $J = 26.1\text{ Hz}$), 49.26 (d, PCH_2N , $J = 27.3\text{ Hz}$), 55.23 (OCH_3), 61.93 (s, NCH_2N), 67.18 (s, NCH_2N), 113.99 (ArC), 133.45 (ArC), 169.68 (s, C = O), 170.11 (s, C = O), C \equiv C signals not observed; ³¹P-NMR (CDCl_3): 1.64 (s); MS(EI): 591.12 [M + H]⁺; elemental analysis [found/theor.]: C(38.59/38.79), H(4.11/4.16), N(7.80/7.54). Complex **4**, [tri[1,3,5-triaza-7-phosphaadamantane]phosphane][2-(4-methoxyphenyl)ethynyl]gold(I). General method: 18.6 mg (0.140 mmol) 1-ethynyl-4-methoxybenzene, 7.9 mg (0.140 mmol) KOH, 10 ml methanol + 5.0 ml dichloromethane, 54.8 mg 381



Fig. 6. NCI-H460 xenograft mice treated with 6 dosages (2.5 mg/kg) of nanoformulated **1** after 14 days.

(0.140 mmol) chloridogold(I)[tri(1,3,5-triaza-7-phosphaadamantane)] phosphane]; 2 h reaction time (then concentrated in vacuum), 12 h at -20°C , yield 10 mg (14%) white powder; $^1\text{H-NMR}$ (CDCl_3): 3.71 (3 H, s, OCH_3), 4.18 (6 H, s, NCH_2N), 4.46 (6 H, m, NCH_2P), 6.72 (2 H, m, ArH), 7.30 (2 H, m, ArH); $^{31}\text{P-NMR}$ (CDCl_3): $-12.61(\text{s})$, MS(ESI) (m/z): 486.10 $[\text{M} + \text{H}]^+$ elemental analysis [found/theor.]: C(37.01/37.13), H(4.13/3.95), N(8.90/8.66).

Complex **5**, (triethylphosphane)[2-(4-methoxyphenyl)ethynyl] gold(I).

General method: 32.6 mg (0.246 mmol) 1-ethynyl-4-methoxybenzene, 41.5 mg (0.768 mmol) KOH, 4.0 ml methanol, 86.5 mg (0.246 mmol) chloridogold(I)(triethylphosphane); 18 h reaction time, 72 h at -20°C , yield 12 mg (11%) gray powder (m.p. $79-80^{\circ}\text{C}$); $^1\text{H NMR}$ (CDCl_3): 1.20 (m, 9 H, $-\text{CH}_3$), 1.80 (m, 6 H, PCH_2); 3.78 (s, 3 H, OCH_3); 6.78 (m, 2 H, ArH), 7.43 (m, 2 H, ArH); $^{13}\text{C NMR}$ (CDCl_3): 8.92 (CH_3), 17.86 (d, CH_2 , $J = 33.0$ Hz), 55.16 (OCH_3), 113.57 (ArC), 117 (ArC), 133.67 (ArC), 158.41 (ArC), $\text{C} \equiv \text{C}$ signals not observed; $^{31}\text{P-NMR}$ (CDCl_3): 38.62 (s); MS(EI): 446.1 $[\text{M} + \text{H}]^+$; elemental analysis [found/theor.]: C(40.65/40.37), H(4.78/4.97).

Complex **6**, [2-(4-methoxyphenyl)ethynyl](trimethylphosphane) gold(I) [42].

General method: 20.62 mg (0.156 mmol) 1-ethynyl-4-methoxybenzene, 26.26 mg (0.468 mmol) KOH, 7.2 ml methanol, 48.13 mg (0.156 mmol) chloridogold(I)trimethylphosphane; 2 h reaction time, overnight at -20°C ; yield: 49.6 mg (79%) light yellow crystals (m.p. $129-132^{\circ}\text{C}$); $^1\text{H NMR}$ (CDCl_3 , 400 MHz): 1.52 (d, $J^2 = 10.1$ Hz, 9 H, P-CH_3); 3.78 (s, 3 H, $-\text{OCH}_3$), 6.78 (m, 2 H, ArH), 7.41 (m, 2 H, ArH); $^{13}\text{C NMR}$ (CDCl_3 , 400 MHz): 15.72 (d, $J = 36.1$ Hz, $-\text{CH}_3$), 55.54 (OCH_3), 113.49 (ArC), 117.20 (ArC), 133.92 (ArC), 158.35 (ArC), $\text{C} \equiv \text{C}$ signals not observed; $^{31}\text{P-NMR}$ (CDCl_3 , 400 MHz): 1.84 (s); MS(EI): 404.1 $[\text{M} + \text{H}]^+$; elemental analysis [found/theor.]: C(35.62/35.66), H(3.92/3.99).

3.4. Computational chemistry

Geometries of all complexes were calculated using the DFT functional PBE [43–46] in conjunction with the Resolution of Identity (RI) [47,48] technique and the def2-TZVPP [32] basis set in vacuo and in water, simulated by the COSMO [49] solvent model. Dispersive interactions were included via Grimme's atom-pair wise dispersion correction [50] (D3) with Becke–Johnson damping (BJ). The stationary point was confirmed as minimum, by a frequency analysis. Bond dissociation scans (10 points) for a bond elongation of 5 Å were performed using LPNO–CEPA/1 [31,51,52] with the def2-QZVP [32]

basis set on gold and def2-TZVP [32] on all other atoms. The solvent (water) was again simulated by the COSMO solvent model. After an elongation of 5 Å the energies did not change significantly any longer and the differences were used as bond dissociation energy. All quantum mechanical calculations were performed using ORCA (version 3.03) [53].

3.5. Cell culture

HT-29 colon carcinoma cells and L-929 mouse fibroblasts were maintained in Dulbecco's Modified Eagle Medium (4.5 g/L D-Glucose, L-Glutamine, Pyruvate), which was supplemented with gentamycin (12.5 mg/L) and fetal bovine serum (Biochrom GmbH, Berlin) (10% V/V), and were passaged once a week. RC-124 healthy human kidney cells were maintained in McCoy's 5A (modified, with L-Glutamine) medium, which was supplemented with gentamycin (12.5 mg/L) and fetal bovine serum (Biochrom GmbH, Berlin) (10% V/V), and were also passaged once a week. For experiments with RC-124 cells, microtiter plates had been pretreated in the following way: 30 μL of a sterilized gelatine solution (1.5% (m/V)) were added to each well of flat bottom 96-well plates, the plates were covered with their lids, incubated for 1 h at 37°C , the excess solution was removed, the wells were washed with PBS 7.4 pH, and the new cell-culture medium was added. 175 cm^2 cell culture flasks used for cultivation of RC-124 cells were pretreated analogously.

3.6. Cell proliferation inhibition (crystal violet assay)

A volume of 100 μL of HT-29 cells (2565 cells/ml), L-929 cells (8100 cells/ml) or RC-124 cells (1460 cells/ml) was transferred into the wells of 96-well plates (note: for RC-124 pretreated plates were used, see above) and incubated at $37^{\circ}\text{C}/5\% \text{CO}_2$ for 48 h (HT-29, L-929) or 72 h (RC-124). Stock solutions of the compounds in dimethylformamide (DMF) were freshly prepared and diluted with the respective cell culture medium to graded concentrations (final concentration of DMF: 0.1% V/V). After 72 h (HT-29, L-929) or 96 h (RC-124) of exposure, the cell biomass was determined by crystal violet staining and the IC_{50} value was determined as the concentration that caused 50% inhibition of cell proliferation compared to an untreated control. Results were calculated as the mean of three independent experiments.

462 3.7. TrxR inhibition

463 The inhibition of isolated rat TrxR was determined as described in
464 previous reports [9,15,33]. IC₅₀ values were calculated from 2–3 inde-
465 pendent experiments and are indicated as mean values with standard
466 errors.

467 3.8. Microscopic live cell imaging

468 RC-124 cells or HT-29 cells were grown in 175 cm² cell culture flasks
469 (gelatine pretreated flasks were used in case of RC-124 cells, see above)
470 as described above until at least 30% confluency. The compounds were
471 prepared freshly as stock solutions in DMF and diluted 1:1000 with
472 cell culture medium. The cell culture medium of the flasks was replaced
473 with fresh medium containing the test compounds at the indicated con-
474 centration. Imaging was performed using a JuLIbR live cell movie analyzer
475 (NanoEnTek) equipped with two microscope units. In each
476 experiment one microscope unit was used to monitor an untreated control
477 and one microscope unit was used to monitor the respective drug
478 treated cells. The microscope units were placed in a CO₂-incubator,
479 loaded with the respective tissue culture flasks, and images were
480 taken in 1 h intervals for a period of 96 h. Each experiment was per-
481 formed twice on separate days and afforded comparable results.

482 3.9. ELISA microarrays

483 Proteins were quantified using sandwich ELISA microarrays. The micro-
484 arrays are based on the ArrayStrip™ platform (Alere Technologies
485 GmbH, Jena, Germany). A detailed description of the assay protocol
486 has been previously reported [54]. Briefly, HT-29 colon carcinoma cells
487 (ATCC) were cultivated at standard cell growth conditions and treated
488 with the indicated concentration of the compound freshly dissolved in
489 dimethylformamide (DMF). For mock-treatment, cells were incubated
490 with the solvent control containing the same amount of DMF as the
491 samples (0.1%). Cells were collected at indicated time points and total
492 protein concentration was determined in cell lysates using the BCA Protein
493 Assay (Pierce Biotechnology, Rockford, USA). Cellular samples were
494 incubated with the microarrays for 60 min. A detection cocktail of 15
495 biotin-labeled phospho-specific detection antibodies (R&D Systems)
496 was used, with the concentration of each antibody at 18 ng/ml. Colorimetric
497 signals were detected by transmission measurements with the Arraymate™
498 reader (Alere Technologies GmbH). Total protein concentrations were used
499 for normalization.

500 3.10. Formulation of **1**

501 For the screening experiments, nine colloidal dispersions were pre-
502 pared: The nanoemulsions contained 10% of the respective oil (soybean
503 oil, refined peanut oil, refined castor oil, Miglyol 812® (all Ph. Eur.),
504 Dynasan® 110 (Hüls AG), Dynasan® 112 (Condea)) and the aqueous
505 phase, which consisted of 5% poloxamer 188 (Kolliphor® P188; BASF)
506 as emulsifier and 2.25% glycerol as isotonicizing agent dissolved in
507 bidistilled water. Mixing of the lipid and aqueous phase by Ultra-
508 Turrax-vortexing and processing in a high pressure homogenizer
509 (Microfluidizer M110-PS, Microfluidics) resulted in nanoemulsions
510 (the solid triglycerides Dynasan® 110 and Dynasan® 112 were pro-
511 cessed at 45 °C and 55 °C respectively, i.e. above their melting tempera-
512 ture). The median particle size was measured using laser diffraction
513 with PIDS technology (Beckman Coulter LS13320) and was below
514 160 nm in all emulsions. Smectic cholesteryl myristate particles were
515 analogously prepared (2.5% cholesteryl myristate (TCI), 2% poloxamer
516 188; median particle size 134 nm) at 95 °C. Mixed micelles were pre-
517 pared by vigorous shaking of 13.4% of the phospholipid Lipoid S100®
518 (Lipoid GmbH) and 7.4% sodium glycocholate hydrate (Sigma) in phos-
519 phate buffer pH 7.4 until translucent. For the liposomes, 15% of Lipoid
520 S100® dispersed in phosphate buffer pH 7.4 was extruded 21 times

through a 100 nm PC membrane. The liposomes had a median size of 521
118 nm. Each preformed carrier was incubated with excess of **1** on a 522
vertical shaker at 20 °C for 10 days. Then, undissolved **1** was filtered 523
off and the dispersions were subjected to AAS measurements. All carriers 524
retained their initial particle size during the screening 525
experiments. 526

Two batches of peanut oil nanoemulsion for the animal studies were 527
prepared separately as described above (median particle size around 528
130 nm). For loading, approximately 1 mg of crushed **1** was incubated 529
with 1 ml of this sterile filtered nanoemulsion under nitrogen atmo- 530
sphere in sterile glass vials. Following one week of incubation, undis- 531
solved material was removed by filtration through a 0.22 µm sterile 532
filter. Finally, the drug-loaded as well as unloaded nanoemulsion (sol- 533
vent control) were filtered (0.22 µm) into heat sterilized glass vials 534
and flushed with sterile filtered nitrogen. All bottling steps were carried 535
out under a clean bench. 536

537 3.11. Atomic absorption spectroscopy (AAS)

Sample preparation was done as follows. Samples: to 180 µL of the 538
respective drug-loaded nanodispersion each 20 µL twice distilled 539
water, Triton X-100 (1%) and ascorbic acid (1%) were added; standard 540
solutions containing **1** were prepared analogously using drug-free 541
nanodispersion and aqueous suspensions of **1** instead of distilled 542
water (matrix matched calibration). The gold levels were measured 543
using a high-resolution continuum source atomic absorption spectrom- 544
eter (ContrAA 700, AnalytikJena AG). For this purpose a volume of 25 µL 545
of the respective sample or standard solution was injected into a stan- 546
dard graphite tube, thermally processed according to an established fur- 547
nace program [19,33], and absorbances were read at 242.7950 nm for 548
5 s. All samples were measured in triplicate and the mean values were 549
used for further calculations. 550

551 3.12. NCI-H460 xenograft experiments

Three and a half million NCI-H460 cells suspended in 100 µL of PBS 552
were injected into the right back flanks of female 4–5 week old BALB/ 553
cAnN-nu (Nude) mice by subcutaneous injection. When the tumor vol- 554
umes reached about 50–100 mm³ (2 days after tumor inoculation), the 555
mice were randomly divided into 2 groups. Solvent control (refined 556
peanut oil nanoemulsion) or 2.5 mg/kg formulated **1** were injected 557
into the mice by intratumoral injection at days 0, 2, 5, 7, 9, 12 (6 doses 558
in total) after treatment. Tumor volumes were measured. None of the 559
mice died during the experiment. They were sacrificed on day 14 after 560
treatment. 561

562 Acknowledgments

The support by COST action CM1105, Deutsche Forschungs- 563
gemeinschaft (DFG), Deutscher Akademischer Austauschdienst (DAAD), 564
and the state of Lower Saxony (graduate program SynFoBiA) as well as 565
technical assistance by Petra Lippmann are gratefully acknowledged. Fi- 566
nancial support of M. K. by a POSTUP2 grant (European Social Fund in 567
the Czech Republic, European Union, Czech ministry of education and 568
sports, operational program for the advancement of the competitive ca- 569
pacity) is gratefully acknowledged (CZ.1.07/2.3.00/30.0041). 570

571 Appendix A. Supplementary data

Supplementary data to this article can be found online at <http://dx.doi.org/10.1016/j.jinorgbio.2015.12.020>. 572
573

574 References

- [1] R. Rubbiani, B. Wahrig, I. Ott, J. Biol. Inorg. Chem. 19 (2014) 961–965. 575
[2] W.F. Kean, I.R. Kean, Inflammopharmacology 16 (2008) 112–125. 576

- 577 [3] T. Zou, C.T. Lum, C.N. Lok, J.J. Zhang, C.M. Che, *Chem. Soc. Rev.* 44 (2015) 8786–8801.
- 578 [4] B. Bertrand, A. Casini, *Dalton Trans.* 43 (2014) 4209–4219.
- 579 [5] I. Ott, *Coord. Chem. Rev.* 253 (2009) 1670–1681.
- 580 [6] S. Nobili, E. Mini, I. Landini, C. Gabbiani, A. Casini, L. Messori, *Med. Res. Rev.* 30 (2010) 550–580.
- 581 [7] T.V. Serebryanskaya, A.S. Lyakhov, L.S. Ivashkevich, J. Schur, C. Frias, A. Prokop, I. Ott, *Dalton Trans.* 44 (2014) 1161–1169.
- 582 [8] Y. Hokai, B. Jurkowicz, J. Fernandez-Gallardo, N. Zakirkhodjaev, M. Sanau, T.R. Muth, M. Contel, *J. Inorg. Biochem.* 138 (2014) 81–88.
- 583 [9] R. Rubbiani, L. Salassa, A. de Almeida, A. Casini, I. Ott, *ChemMedChem* 9 (2014) 1205–1210.
- 584 [10] O. Rackham, S.J. Nichols, P.J. Leadman, S.J. Berners-Price, A. Filipovska, *Biochem. Pharmacol.* 74 (2007) 992–1002.
- 585 [11] M. Frik, J. Jimenez, I. Gracia, L.R. Falvello, S. Abi-Habib, K. Surriel, T.R. Muth, M. Contel, *Chem. Eur. J.* 18 (2012) 3659–3674.
- 586 [12] K.H.-M. Chow, R.W.-Y. Sun, J.B.B. Lam, C.K.-L. Li, A. Xu, D.-L. Ma, R. Abagyan, Y. Wang, C.-M. Che, *Cancer Res.* 70 (2010) 329–337.
- 587 [13] G. Boscutti, L. Marchio, L. Ronconi, D. Fregona, *Chem. Eur. J.* 19 (2013) 13428–13436.
- 588 [14] M.N. Kouodom, G. Boscutti, M. Celegato, M. Crisma, S. Sitran, D. Aldinucci, F. Formaggio, L. Ronconi, D. Fregona, *J. Inorg. Biochem.* 117 (2012) 248–260.
- 589 [15] R. Rubbiani, E. Schuh, A. Meyer, J. Lemke, J. Wimberg, N. Metzler-Nolte, F. Meyer, F. Mohr, I. Ott, *Med. Chem. Commun.* 4 (2013) 942–948.
- 590 [16] J.L. Hickey, R.A. Ruhayel, P.J. Barnard, M.V. Baker, S.J. Berners-Price, A. Filipovska, *J. Am. Chem. Soc.* 130 (2008) 12570–12571.
- 591 [17] T. Zou, C.T. Lum, C.-N. Lok, W.-P. To, K.-H. Low, C.-M. Che, *Angew. Chem. Int. Ed.* 53 (2014) 5810–5814.
- 592 [18] B. Bertrand, A. Citta, I.L. Franken, M. Picquet, A. Folda, V. Scalcon, M.P. Rigobello, P. Le Gendre, A. Casini, E. Bodio, *J. Biol. Inorg. Chem.* 20 (2015) 1005–1020.
- 593 [19] A. Meyer, C.P. Bagowski, M. Kokoschka, M. Stefanopoulou, H. Alborzina, S. Can, D.H. Vlecken, W.S. Sheldrick, S. Wölfl, I. Ott, *Angew. Chem. Int. Ed.* 51 (2012) 8895–8899.
- 594 [20] R.G. Balasingham, C.F. Williams, H.J. Mottram, M.P. Coogan, S.J.A. Pope, *Organometallics* 31 (2012) 5835–5843.
- 595 [21] E. Schuh, S.M. Valiahdi, M.A. Jakupec, B.K. Keppler, P. Chiba, F. Mohr, *Dalton Trans.* (2009) 10841–10845.
- 596 [22] E. Vergara, E. Cerrada, A. Casini, O. Zava, M. Laguna, P.J. Dyson, *Organometallics* 29 (2010) 2596–2603.
- 597 [23] J.C. Lima, L. Rodriguez, *Chem. Soc. Rev.* 40 (2011) 5442–5456.
- 598 [24] J. Arcau, V. Andermark, E. Aguilo, A. Gandioso, A. Moro, M. Cetina, J.C. Lima, K. Rissanen, I. Ott, L. Rodriguez, *Dalton Trans.* 43 (2014) 4426–4436.
- 599 [25] E.E. Langdon-Jones, D. Lloyd, A.J. Hayes, S.D. Wainwright, H.J. Mottram, S.J. Coles, P.N. Horton, S.J. Pope, *Inorg. Chem.* 54 (2015) 6606–6615.
- 600 [26] L. Massai, J. Fernandez-Gallardo, A. Guerri, A. Arcangeli, S. Pillozzi, M. Contel, L. Messori, *Dalton Trans.* 44 (2015) 11067–11076.
- 601 [27] J. Fernandez-Gallardo, B.T. Elie, F.J. Sulzmaier, M. Sanau, J.W. Ramos, M. Contel, *Organometallics* 33 (2014) 6669–6681.
- 602 [28] A. Debnath, D. Parsonage, R.M. Andrade, C. He, E.R. Cobo, K. Hirata, S. Chen, G. Garcia-Rivera, E. Orozco, M.B. Martinez, S.S. Gunatilleke, A.M. Barrios, M.R. Arkin, L.B. Poole, J.H. McKerrow, S.L. Reed, *Nat. Med.* 18 (2012) 956–960.
- 603 [29] J.M. Madeira, D.L. Gibson, W.F. Kean, A. Klegeris, *Inflammopharmacology* 20 (2012) 297–306.
- 604 [30] A. Meyer, A. Gutiérrez, I. Ott, L. Rodríguez, *Inorg. Chim. Acta* 398 (2013) 72–76.
- 605 [31] F. Neese, F. Wennmohs, A. Hansen, *J. Chem. Phys.* 130 (2009) 114108.
- 606 [32] F. Weigend, R. Ahlrichs, *Phys. Chem. Chem. Phys.* 7 (2005) 3297–3305.
- 607 [33] R. Rubbiani, S. Can, I. Kitanovic, H. Alborzina, M. Stefanopoulou, M. Kokoschka, S. Mönchgesang, W.S. Sheldrick, S. Wölfl, I. Ott, *J. Med. Chem.* 54 (2011) 8646–8657.
- 608 [34] A. Bindoli, M.P. Rigobello, G. Scutari, C. Gabbiani, A. Casini, L. Messori, *Coord. Chem. Rev.* 253 (2009) 1692–1707.
- 609 [35] A. Pratesi, C. Gabbiani, E. Michelucci, M. Ginanneschi, A.M. Papini, R. Rubbiani, I. Ott, L. Messori, *J. Inorg. Biochem.* 136 (2014) 161–169.
- 610 [36] M.P. Rigobello, G. Scutari, A. Folda, A. Bindoli, *Biochem. Pharmacol.* 67 (2004) 689–696.
- 611 [37] P. Holenya, I. Kitanovic, F. Heigwer, S. Wolf, *Proteomics* 11 (2011) 2129–2133.
- 612 [38] E. Kupetz, L. Preu, C. Kunick, H. Bunjes, *Eur. J. Pharm. Biopharm.* 85 (2013) 511–520.
- 613 [39] U. Jungwirth, J. Gojo, T. Tuder, G. Walko, M. Holcman, T. Schofl, K. Nowikovsky, N. Wilfinger, S. Schoonhoven, C.R. Kowol, R. Lemmens-Gruber, P. Heffeter, B.K. Keppler, W. Berger, *Mol. Cancer Ther.* 13 (2014) 2436–2449.
- 614 [40] P. Holenya, S. Can, R. Rubbiani, H. Alborzina, A. Junger, X. Cheng, I. Ott, S. Wolf, *Metalomics* 6 (2014) 1591–1601.
- 615 [41] X. Cheng, P. Holenya, S. Can, H. Alborzina, R. Rubbiani, I. Ott, S. Wolf, *Mol. Cancer* 13 (2014) 221.
- 616 [42] V.W.-W. Yam, S.W.-K. Choi, *Dalton Trans.* (1996) 4227–4232.
- 617 [43] J.C. Slater, *Phys. Rev.* 81 (1951) 385–390.
- 618 [44] J.P. Perdew, K. Burke, M. Ernzerhof, *Phys. Rev. Lett.* 77 (1996) 3865–3868.
- 619 [45] J.P. Perdew, K. Burke, Y. Wang, *Phys. Rev. B* 54 (1996) 16533–16539.
- 620 [46] P.A.M. Dirac, *Proc. R. Soc.* 123 (1929) 714–733.
- 621 [47] K. Eichkorn, O. Treutler, H. Öhm, M. Häser, R. Ahlrichs, *Chem. Phys. Lett.* 242 (1995) 652–660.
- 622 [48] O. Vahtras, J. Almlöf, M.W. Feyereisen, *Chem. Phys. Lett.* 213 (1993) 514–518.
- 623 [49] A. Klamt, G. Schürmann, *J. Chem. Soc. Perkin Trans.* 2 (1993).
- 624 [50] S. Grimme, J. Antony, S. Ehrlich, H. Krieg, *J. Chem. Phys.* 132 (2010) 154104.
- 625 [51] V. Staemmler, R. Jaquet, *Theor. Chim. Acta* 59, 181, pp. 487–500.
- 626 [52] R. Ahlrichs, *J. Chem. Phys.* 62 (1975) 1225.
- 627 [53] F. Neese, *Interdiscip. Rev. Comput. Mol. Sci.* 2 (2012) 73–78.
- 628 [54] P. Holenya, F. Heigwer, S. Wolf, *J. Immunol. Methods* 380 (2012) 10–15.